Free-Wave Energy Dissipation in Experimental Breaking Waves

EUSTORGIO MEZA AND JUN ZHANG

Ocean Engineering Program, Department of Civil Engineering, Texas A&M University, College Station, Texas

RICHARD J. SEYMOUR

*Ocean Engineering Research Group, Scripps Institution of Oceanography, University of California, San Diego,
La Jolla, California*

ABSTRACT

Several transient wave trains containing an isolated plunging or spilling breaker at a prescribed location were generated in a two-dimensional wave flume using an energy focusing technique. Surface elevation measurements of each transient wave train were made at locations before and after breaking. Applying a nonlinear deterministic decomposition approach to the measured elevation, the free-wave components of the transient wave train were derived by excluding the contribution from bound-wave components. The comparison of the amplitude or energy spectra of free-wave components before and after a breaker can accurately reveal the energy dissipation as a function of frequency. It is found that the energy loss is almost exclusively from wave components at frequencies higher than the spectral peak frequency. Although the energy density of the wave components of frequencies near the peak frequency is the largest, they do not significantly gain or lose energy after the breaking. It is also observed that wave components of frequencies significantly below or near the peak frequency gain a small portion (about 12%) of energy lost by the high-frequency waves. These findings are quite different from the empirical formulas presently used for determining wave dissipation due to wave breaking. Hence, they have important implications to the ocean wave energy budget, specially to the energy transfer at frequencies below and near the spectral peak frequency.

1. Introduction

Although wave energy is eventually dissipated in shallow waters and on beaches, wave breaking plays a dominant role in dissipating ocean surface wave energy in deep and intermediate-depth water (Anis and Moum 1995; Terray et al. 1996; Drennan et al. 1996). Better understanding of wave breaking is crucial to the prediction of wind-driven wave spectra (WAMDI Group 1988). Present understanding of energy dissipation resulting from wave breaking is far from adequate and its estimate is inaccurate (Phillips 1984; Komen et al. 1984, 1994; Melville 1996). While wave energy at a given frequency may be reduced owing to wave breaking, at the same time its energy may also change due to the input from wind and the energy transfer to or from waves of different frequencies. Hence, direct measurements of energy dissipation due to wave breaking in the sea is extremely difficult. As an alternative, the dissi-

pation of wave breaking is often measured and investigated in laboratories. An irregular wave train can be generated by a computer-controlled wavemaker in a two-dimensional (2D) wave flume in such a way that wave energy focuses at a prescribed location and results in an isolated breaker. Since no wind is present in the wave flume and the energy transfer among different wave frequencies is negligible owing to the small length scale of the wave breaking, the differences in energy before and after an isolated breaker can be viewed as the dissipation due to wave breaking.

The above laboratory technique was employed by Rapp and Melville (1990), who extensively studied the velocity field induced by different types of isolated breakers and the related losses of momentum and energy. By comparing the spectra measured before and after an isolated breaker, they observed that 1) major energy loss occurs at the "second harmonic" band and slight loss at the higher end of the "first harmonic" band, and 2) the low-frequency waves in all cases studied propagate through breaking, even the intense plunging breaking, without significant loss of energy. The wave train generated in the study of Rapp and Melville (1990) consists of many wave components of different frequencies. The first harmonic and second harmonic

Corresponding author address: Dr. Jun Zhang, Coastal and Ocean Engineering Division, Texas A&M University, Department of Civil Engineering, College Station, TX 77843-3136.
E-mail: jun-zhang@tamu.edu

bands were referred to the frequency bands centered at the spectral peak frequency and twice of that frequency, respectively. They also reported that even though the wave was not breaking, the spectra at different locations changed significantly at high and low frequencies. They attributed these changes to the growth of the forced (or bound) wave components. Later, Melville (1996) pointed out that spectra at low frequency displayed a slight increase downstream of the breaking region. He thought it would be consistent with the generation of free long waves resulting from the change in the gradients of the radiation stress accompanying breaking. The slight energy increase in low-frequency waves implies that breaking is not just a sink of wave energy, but can also be a source to waves of low frequencies. His implication is qualitatively different from the formulation currently used to model energy dissipation in wind-driven ocean waves. The latter considers wave breaking to be an energy sink to all waves, regardless of their frequencies. More recently, Kway et al. (1998) also conducted laboratory studies of wave breaking and obtained similar observations as those of Rapp and Melville. Although important observations of energy dissipation due to wave breaking as a function of frequency have been made and they have important implication to ocean wave models concerning the long-term evolution of a wave spectrum, no effort has been made to quantify the energy loss at high frequencies and to resolve a subtle difference between the observations that the waves of low frequencies propagate through the breaking without significant loss of energy (Rapp and Melville 1990; Kway et al. 1998) and that they slightly gain energy through wave breaking (Melville 1996). If the low-frequency waves do gain energy, then two key questions need to be answered. What is the magnitude of the gain and is it important to wave models concerning the long-term evolution of a wave spectrum? To fill the gap in our knowledge of energy dissipation, this study employs the same laboratory technique to investigate and quantify the energy dissipation as a function of wave frequency caused by various types of isolated breakers. Since the energy gain or loss is very small, specially at the low-frequency band, accurate measurements and computation of wave energy spectra are crucial. A major obstacle in the previous studies for determining the energy dissipation as a function of wave frequency is the significant changes in both high- and low-frequency bands of the wave spectra measured at different locations along a wave flume even in the absence of wave breaking. The changes in wave energy at low- and high-frequency bands due to the presence of bound-wave components can be significant and interfere with the changes due to wave breaking in the same frequency bands. In other words, the presence of bound-wave energy contaminates the measurements of energy loss and gain due to wave breaking if the energy dissipation is determined by a direct comparison of the wave spectra measured before and after a breaker. To overcome this difficulty, the contributions of bound-wave components in the resultant wave elevation must be thoroughly understood and considered separately from those of free-wave components.

2. Decoupling of bound-wave components

An ocean wave field consists of a continuum of monochromatic wave components of different frequencies, amplitudes and advancing in different directions. These basic wave components, known as free-wave (or linear) components, obey the dispersion relation. Due to the nonlinear nature of surface waves, the free-wave components interact among themselves. According to their effects on wave characteristics, the wave–wave interactions can be classified into "strong" and "weak" interactions (Phillips 1979; Sue and Green 1981). The effects of the strong interactions are observable as "bound-wave" components immediately after the interactions start. In contrast to free-wave components, bound-wave components do not obey the dispersion relation. The effects of weak interactions (also known as resonant interactions) may be substantial in a duration of hundreds of wave periods after the interactions start. Through the weak interactions, wave energy is transfered among free-wave components of different frequencies permanently. Hence, the weak interactions are crucial to the long-term evolution of wave spectra, yet negligible to the change of spectra in a short distance, say in a length scale comparable to a single breaker. On the other hand, the effects of strong wave–wave interactions or bound-wave components depend on the interacting free-wave components and exist temporarily (except the second and high harmonics of a free-wave component). That is, when the free-wave components whose interaction results in the bound-wave components no longer travel together, the corresponding bound-wave components disappear (Yuen and Lake 1982). Hence, the energy of bound-wave components is unimportant to the long-term evolution of ocean wave spectra.

When a transient wave train propagates in a 2D flume, the bound-wave components instantaneously change a wave spectrum at very high and low frequencies in two ways. First, far upstream of wave breaking, the free-wave components of different frequencies in the transient wave train have not superposed yet, and thus no strong interactions between these free-wave components occur. When relatively low-frequency free-wave components overtake relatively high-frequency free-wave components near the location of breaking, the strong interactions among them occur and bound-wave components become great. That is why the energy at very high and low frequency bands significantly increases right before the breaking as observed in Rapp and Melville (1990) and Kway et al. (1998). When the low-frequency free-wave components surpass the high-frequency components downstream of breaking, the strong interactions between them disappear and so do the cor-
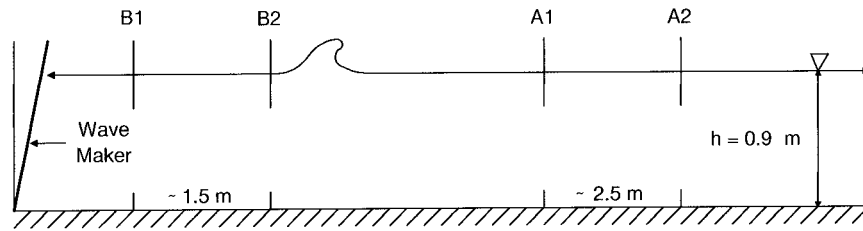
FIG. 1. Sketch of wave gauges for the measurement of transient breaking waves.

responding bound-wave components. The occurrence and disappearance of bound-wave components along the wave flume can make the spectra at different locations quite different. Second, the measured spectra at very high and low frequency bands are the resultant of the free-wave and bound-wave components in these bands. Because the phase velocities of a free-wave and bound-wave component of the same frequency are different, the resultant amplitude (spectrum) at a frequency changes from one location to another even though the amplitudes of the underling free-wave and bound-wave components do not change.

From the view of the long-term evolution of wave spectra, the energy loss and gain of the free-wave components are relevant and the occurrence and disappearance of bound-wave components are irrelevant. To accurately quantify the energy loss and gain due to wave breaking, it is desirable to decouple the contributions of the bound-wave components from the measured elevation. The separation of the bound-wave components from the free-wave components can be accomplished through a nonlinear decomposition of an irregular or transient wave train (Zhang et al. 1996), in which the bound-wave components can be deterministically calculated based on the measured (resultant) wave elevation and then decoupled from the latter. The free-wave components can then be derived using the fast Fourier transform (FFT) based on the modified measured elevation. The free-wave components are assumed to be steady within a short distance and in the absence of breaking. Therefore, the differences in the amplitudes of free-wave components before and after an isolated breaker can accurately reveal the energy loss or gain of free-wave components due to wave breaking.

3. Experiment setup

The experiment was conducted in a 2D wave flume at the Hydromechanics Laboratory of the Civil Engineering Department at Texas A&M University. The flume is 36.1 m in length overall, 0.91 m wide and 1.22 m deep. The water depth during the experiment was 0.91 m. Very steep transient wave trains were formed by sequentially generating a series of waves from high to low frequencies that superposed at a downstream location. The mechanism of generating a transient wave train was similar to that used by Rapp and Melville

(1990). However, our spectra have a sharp peak and constant wave steepness for each free-wave component while their spectra have a ''top hat'' shape with constant amplitude for each free-wave component.

As the wave train propagated along the flume, it became steep due to wave energy focussing and eventually broke as a plunging or spilling breaker. Different types of breakers can be realized by varying the wave steepness of the free-wave components (Krafft and Kim 1987). Four resistance-type surface-piercing wave gauges were used to measure the wave elevation before and after a breaker. The relative positions of the wave gauges in the wave flume are sketched in Fig. 1. The sampling rate of measuring wave elevation was at least 50 Hz. For reference, the location where the wave breaking occurred is also marked. The exact locations of the wave gauges varied slightly in measuring different transient wave trains according to their spectral peak frequencies and types of breakers. Attention was paid to place wave gauge B2 before any breaking occurred and wave gauge A1 about 1.5 to 2.0 m downstream of a breaker where no traces of air entrainment were observed. The wave gauges were calibrated using a linear least squares regression. The standard deviation of the calibration was 0.2 mm. Because the wavemaker is computer-controlled, the transient wave trains can be almost identically repeated. Each of the wave trains were run and measured four times.

4. Measurements and data analysis

a. Characteristics of transient wave trains

In total, 13 different breaking and nonbreaking transient wave trains were generated and measured in the flume. Their main characteristics are listed in Table 1. The letters P, S and N denote a plunging, spilling, and nonbreaking wave train, respectively. Following Rapp and Melville (1990) and Banner and Peregrine (1993), a nonbreaking wave is defined as one where the free surface remains smooth as the wave train propagates through the packet envelope. A spilling breaker is defined as one where the fluid appears to break out of the surface and ''white water'' falls down the front face of the wave. A plunging breaker is defined as one where the breaking commences with wave overturning forming a forward moving sheet of water that curls down into

TABLE 1. Experimental transient breaking waves classified by type of breaking: peak frequency, amplitude, wave steepness before and after the breaking, and wave energy gain to loss ratio. The superscript markers on the wave trains refer to wave trains that were measured by wave gages at the same exact position. σ^2 is the free-wave spectrum variance, ω is the angular peak frequency and g is the acceleration of gravity. E_{gain} and E_{loss} refer, respectively, to the total potential energy gained and lost by the low and high frequency wave components during wave breaking.

Wave train	Peak frequency (Hz)	Peak amplitude (cm)	Wave steepness before $\sigma \frac{\omega^2}{g^{-1}}$	Wave steepness after $\sigma \frac{\omega^2}{g^{-1}}$	Wave energy gain to loss ratio $\dfrac{E_{gain}}{E_{loss}}$
P1*	0.73	2.011	0.0687	0.0520	0.072
P2★	0.73	1.778	0.0584	0.0518	0.127
P3	0.63	2.280	0.0551	0.0483	0.085
P4	0.63	2.044	0.0549	0.0486	0.064
P5	0.53	2.231	0.0392	0.0357	0.129
S1°	0.73	1.611	0.0559	0.0439	0.267
S2•	0.73	1.390	0.0461	0.0430	0.086
S3	0.63	1.351	0.0369	0.0345	0.084
S4	0.53	1.548	0.0278	0.0265	0.170
N1*	0.73	1.342	0.0480	0.0463	
N2★	0.73	1.153	0.0398	0.0384	
N3°	0.73	1.343	0.0473	0.0465	
N4•	0.73	1.150	0.0392	0.0384	

the water. Each breaking transient wave train contained a single breaker. The very steep but nonbreaking wave trains (N1–N4) were, respectively, similar to, but slightly smaller than, the breaking wave trains P1, P2, S1, and S2 in wave elevation. The measurements of the nonbreaking wave trains (N1–N4) were aimed at ex-

amining the magnitude of various errors made in determining energy loss and gain of free-wave components.

For illustrating the measurements and data analysis, the wave train P3 involving a strong plunging breaker is used as an example in the description. A general view of wave elevations of P3 measured before and after the wave breaker are plotted as a function of time in Fig. 2.

The resultant amplitude spectra of the elevations measured before and after a breaker were obtained using the FFT, and are given, respectively, in Figs. 3 and 4. The time series input to the FFT is 20.48 s long (1024 points). The spectral peak frequency of P3 is 0.63 Hz and the wave amplitude above 2.25 Hz is insignificant and thus the spectra are truncated at this frequency. The resultant amplitude spectra are obtained from the FFT of a single time series without making the ensemble average or frequency band merge. Figure 3 shows that the two spectra measured at two different locations be-
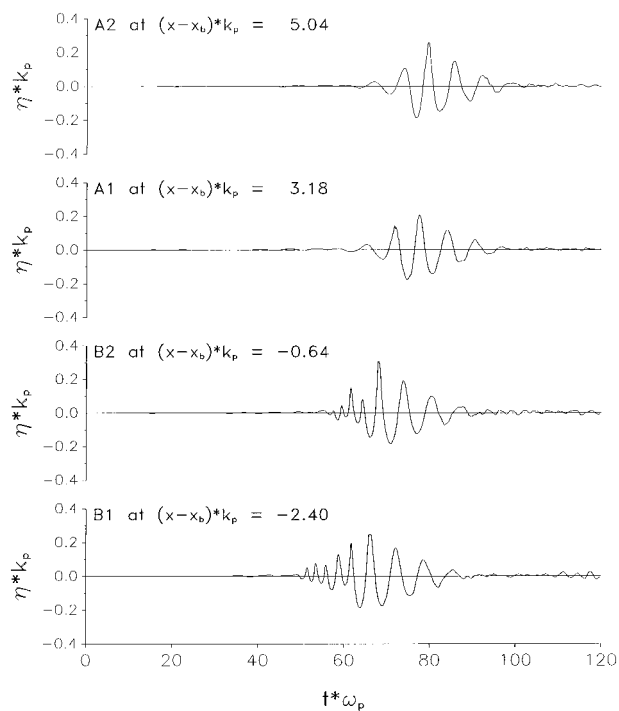

FIG. 2. Time history of surface displacement at various distances from the observed breaking point, x_b. Wave peak parameters $\omega_p = 3.96$ rad s^{-1} and $k_p = 1.74$ m^{-1}. Wave breaking was observed between $(x - x_b)k_p = -0.64$ and 3.18.
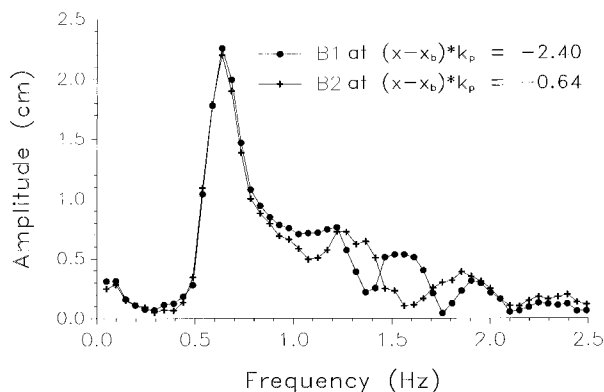

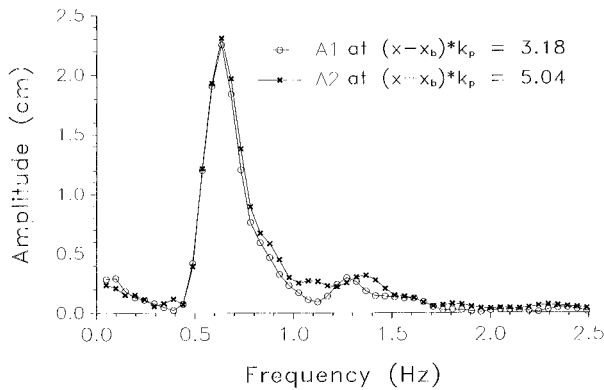FIG. 3. Resultant wave elevation spectra before a plunging breaker.

FIG. 4. Resultant wave elevation spectra after a plunging breaker.

fore the wave breaking are similar overall. Specially, near the peak frequency the amplitudes are almost identical. However, there are large discrepancies within the frequency band (1.00–1.90 Hz) higher than the peak frequency and relatively small discrepancies in the low-frequency band (0.1–0.5 Hz). The high-frequency and low-frequency bands, respectively, correspond to those of the second-order sum-frequency and difference-frequency interactions that result from the interactions between the free-wave components near the peak frequency (0.50–0.95 Hz). Similar features are also observed in Fig. 4 for the two spectra measured after breaking. These observations are similar to those of Rapp and Melville (1990) and Kway et al. (1998).

The resultant amplitude at a given frequency is essentially the superposition of a free-wave component and bound-wave components at the same frequency. Near the spectral peak frequency, the contributions to the resultant amplitude from the free-wave components are dominant while those from the bound-wave components are insignificant. In the absence of breaking (between B1 and B2, and between A1 and A2), they are expected to remain the same because the effects of weak interactions are negligible within a short distance. In the higher frequency (sum-frequency) and very low-frequency (difference-frequency) bands, the contributions from the bound-wave components are comparable to or even greater than those from the free-wave components (Zhang et al. 1996). Consequently, large discrepancies are expected in these frequency bands as elucidated in section 2. The reasons for why the discrepancies in the low-frequency band are much smaller than the counterparts in the high-frequency band are 1) the distance between the two gauges located either before or after breaking is small in comparison with the wavelengths of either free-wave or bound-wave components in the low-frequency band but large in comparison with the those in the high-frequency band, 2) the amplitudes of both bound-wave and free-wave components in the low-frequency band are very small, and 3) various errors made in measuring free-wave components are much greater in the high-frequency band

than in the low-frequency band, which will be further discussed.

b. Computation of free-wave components

The Hybrid wave model (HWM) developed recently by Zhang et al. (1996) allows a deterministic nonlinear decomposition of an irregular wave field. The input to the HWM is a time series of a wave property recorded at a fixed point in the case of a unidirectional irregular wave train. In this study, the measurements of surface elevation were used as the input. Based on the input, the HWM first calculates the bound-wave components and then decouples their effects from the measured elevation. After the decoupling of the bound-wave components, the free-wave components can be obtained from the FFT of the modified measurement. The calculation of bound-wave components, however, needs to know the free-wave components whose strong interactions result in the bound-wave components. Hence, the decomposition of an irregular wave train into free-wave components is accomplished through an iterative procedure that consists of three steps: computation of free-wave components, computation of bound-wave components, and decoupling the bound-wave components from the measurement. The formulation for the computation of bound-wave components in the HWM is accurate at least up to second order in wave steepness. The iterative procedure in the decomposition is found to be convergent when applied to very steep wave trains including irregular wave trains close to breaking (Spell et al. 1996). After the amplitudes and initial phases of the free-wave components in an irregular wave train are obtained, a variety of resultant wave properties, say surface elevation, dynamic pressure and wave-induced particle velocities near the location of measurements can be deterministically predicted by superposing the contribution from free-wave and bound-wave components and allowing for their respective propagation. These predictions are useful to many applications of offshore engineering and ocean wave measurements (Cao and Zhang 1997; Couch and Conte 1997; Meza et al. 1999). In addition, they were employed to examine the accuracy of the HWM. Extensive comparisons between the predicted wave properties obtained using the HWM and the corresponding measurements were made and showed that the HWM is reliable and much more accurate than linear spectral methods and their modifications (Spell et al. 1996; Randall et al. 1993). For more details of the HWM and its results, readers are referred to Zhang et al. (1996) and Spell et al. (1996).

Using the HWM, the amplitudes and initial phases of free-wave components were computed based upon the same elevation measurement used for computing the resultant amplitude spectra. The free-wave amplitude spectra of wave train P3 at locations B1 and B2 (before the breaking) are shown in Fig. 5 and those at locations A1 and A2 (after the breaking) in Fig. 6. It should be
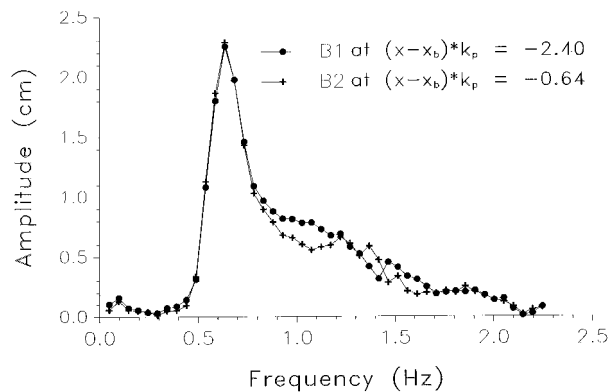
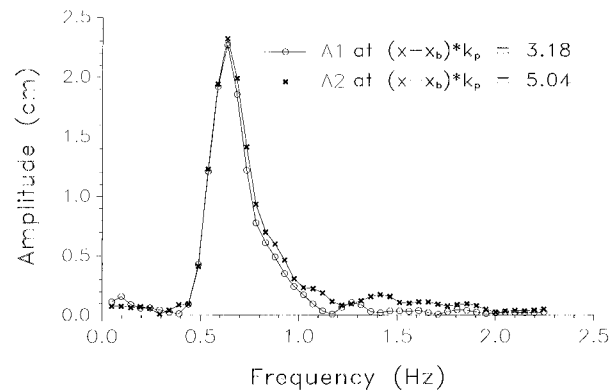FIG. 5. Free wave elevation spectra before a plunging breaker.

FIG. 6. Free wave elevation spectra after a plunging breaker.

noted that the initial phases of the free-wave components are also different from those of the resultant wave components. Since they are irrelevant to energy dissipation, their presentation is omitted.

Figure 5 shows that the two free-wave amplitude spectra measured at two different locations before the breaking are very close not only in the frequency band close to the peak frequency but in the low- and high-frequency bands as well. In comparison, the two corresponding resultant amplitude spectra shown in Fig. 3 are very close only at frequencies near the spectral peak, but show substantial differences in the high-frequency band. As mentioned previously, the differences in the high-frequency band of the resultant amplitude spectra are due to the presence of bound-wave components resulting from the strong (sum-frequency) interactions. In the free-wave amplitude spectra, the corresponding contributions of bound-wave components are excluded and the spectra are hence very similar in the entire frequency range. The same trend is observed in the comparison between the two spectra of free-wave amplitudes at locations after the breaking (Fig. 6). However, it is noticed that there still exist small discrepancies mainly in the high-frequency band between the two free-wave amplitude spectra in Figs. 5 and 6. These differences are due to the errors made in measuring and determining the free-wave components. The magnitude of errors are discussed below.

c. Magnitude of errors

Five types of errors (or uncertainties) exist in measuring wave elevation and determining free-wave amplitudes. They are

1) errors in measuring wave elevation,
2) errors resulting from inexact repeat of a transient wave train in different runs,
3) errors due to the presence of transverse waves in the flume,
4) neglect of viscous effects due to the side walls and bottom of the flume, and

5) neglect of bound wave components of third order or higher in wave steepness.

The first three errors are related to the measurements and experiment facility and the last two to the assumptions made in the analysis.

The calibration of the wave gauges indicates that the errors in measuring wave elevation have a standard deviation ($\sigma = 0.2$ mm). These errors are approximated as random errors of a normal distribution ($\sigma = 0.2$ mm and mean $= 0$). It should be noted that the error in each discrete elevation data is different from the error of a resultant wave amplitude obtained using the FFT. A wave component of period T involves n ($=T/\delta t$) discrete sampling elevation data in one period, where δt is the time increment between two neighboring sampling data and equal to 0.02 s (50 Hz) in most of our measurements. Assuming the random error of each discrete elevation data is independent of that of other elevation data, they remain independent after multiplying by the weighting function of the FFT (whose modulus is unity). Noticing that the amplitude of a wave component of period T (Fourier coefficient) is obtained through averaging n elevation data multiplying by the FFT weighting function, the error of the wave amplitude is hence an average of the individual errors of the n data. Following the central limit theorem, the error of the resultant wave amplitude of period T has a normal distribution of a standard deviation $\sigma_T = \sigma/\sqrt{n}$. For $T = 2$ s, its standard deviation is 0.02 mm. Further, the duration of the elevation time series used in the FFT is many times of T and the actual error becomes even smaller than the above estimate.

The repeatability of a transient wave train in a flume depends on the precision of its wave generation facility. It is examined by comparing the resultant amplitude spectra of different runs but measured at the same location. Since the spectra are calculated from a measured elevation using the FFT, the measurement errors are also included in the difference between the two spectra of different runs. Figure 7 plots the resultant amplitude spectra for two different runs of the breaking wave train
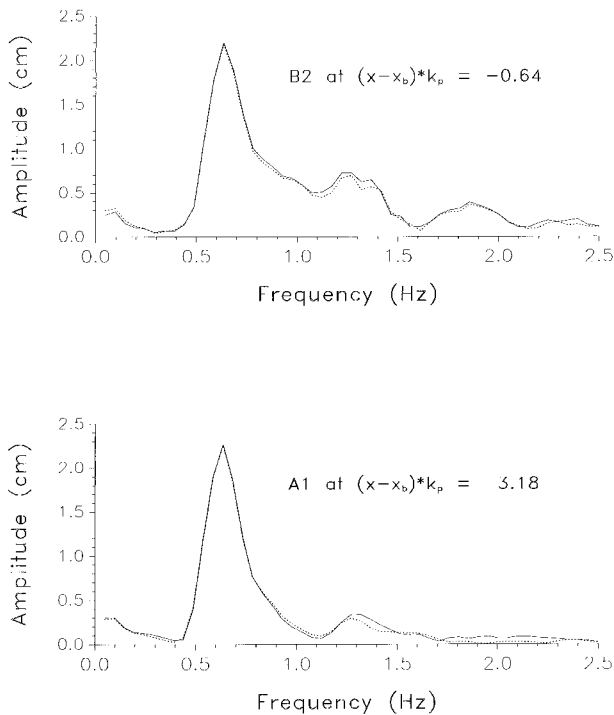
FIG. 7. Resultant wave elevation spectra of two different runs at a fixed location before (B2) and after (A1) a plunging breaker.

P3 at the locations B2 and A1, respectively. The figure shows that the resultant wave spectra of two different runs are almost identical, indicating that repeatability of wave trains is satisfactory. The differences between the two spectra of different runs are very small, especially in the low-frequency band, which also indirectly confirms that the measurement errors at the low-frequency band are indeed small. The discrepancies, however, in the high-frequency band is much greater. The large discrepancies in the high-frequency band are due mainly to the transverse waves generated in the flume.

When a transient wave train advancing in a flume is steep, transverse waves will be generated. The wave flume is 0.91 m wide and the water depth during the tests was 0.91 m. Thus the first six modes of the transverse waves have the natural frequencies of 0.92, 1.31, 1.60, 1.85, 2.07, and 2.26 Hz, in sequence. Different from free and bound waves, the transverse waves do not advance in the flume and in general they superpose on the surface of a wave train differently in different runs and in different locations. As shown in Fig. 7, at the same location (either B2 or A1), the largest differences between the spectra of different runs occur at the frequencies near those natural frequencies of transverse waves. The presence of the transverse waves is found to be the major cause that the errors are much greater in the high-frequency band than in the low-frequency band. It is also responsible for the relatively large discrepancies in the high-frequency band of the free-wave

spectra of the same run but obtained in different locations (see Figs. 5 and 6).

The viscous effects of the side walls and bottom of a flume are expected to reduce the wave energy downstream. However, the longest distance between any two wave gauges in all measurements is less than 9 m. Because the wave gauges were placed in the middle of the flume, the reduction due to viscous effects on the amplitudes of wave components in the frequency range that we are interested in is insignificant.

Finally, the high-order bound waves (third order or higher) cannot be extracted from the measurements using the HWM. Hence, they result in errors when comparing free-wave amplitude spectra obtained at different locations. The last two types of errors are expected to be small in comparison with the errors caused by the transverse waves.

To quantify the magnitude of total errors described above, the measurements of nonbreaking transient wave trains were made. The nonbreaking wave trains (N1–N4) are very steep and resemble the breaking wave trains (P1, P2, S1, and S2) in the elevation profile but of slightly smaller amplitudes. The free-wave amplitude spectra were obtained from their elevation measurements using the HWM as those of breaking wave trains. The wave gauges for measuring nonbreaking wave trains were deliberately placed in the same locations for measuring the breaking wave trains. Because there is no wave breaking between two wave gauges (say, B2 and A1) in the case of nonbreaking wave trains, the differences in the free-wave amplitude spectra of a nonbreaking wave train obtained at different locations are considered as the errors. The magnitude of the differences is hence an indicator of total errors discussed above. The amplitude-difference spectra of four nonbreaking wave trains (N1 to N4) are given in Fig. 8. The difference spectrum of a nonbreaking wave train was obtained by subtracting the average of its free-wave spectra at A1 and A2 of four runs from that of B1 and B2. The frequency in Fig. 8 is normalized by the corresponding spectral peak frequency. The figure shows that the amplitude differences overall are small. The magnitude of the errors is very small (0.1–0.2 mm) in the low-frequency range (f/f_p = 0.8–0.9) and relatively small (0.5–1.0 mm) in the high-frequency range (f/f_p = 1.1–2.0). The results are consistent with the analysis regarding the magnitude of errors in the different frequency bands. Although the magnitude of errors in different frequency bands shown in Fig. 8 belongs to nonbreaking wave trains, we expect the related error magnitude in measuring breaking wave trains is of the same order. It will be shown in the next section that the measured energy loss and gain of breaking wave trains is of order of 1.0 mm in the low-frequency band and of order of 2–5 mm in the high-frequency band, which are much greater than the errors in the respective frequency bands. Further, the trend of errors shown in the nonbreaking wave trains is quite different from that of gain
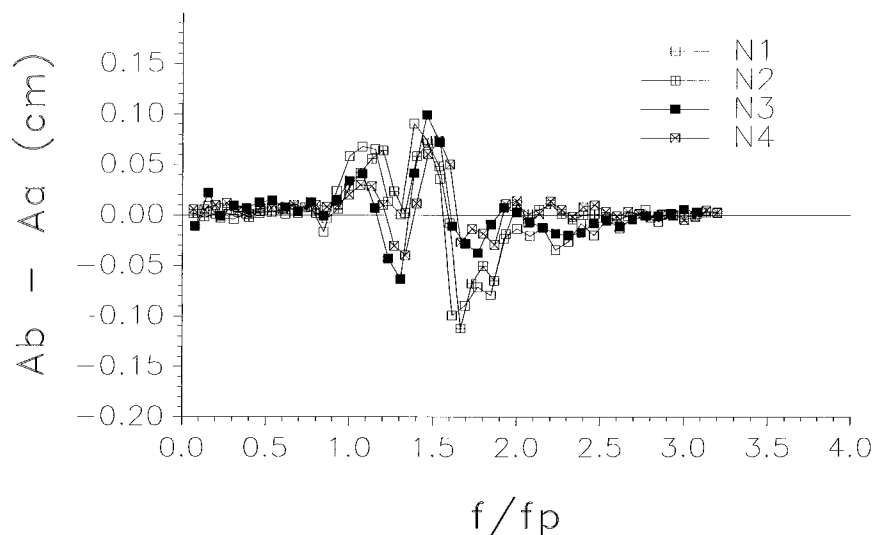
FIG. 8. Free-wave amplitude-difference spectra for very steep nonbreaking wave trains of Table 1: Ab and Aa are, respectively, the average free-wave amplitude spectra before and after breaking, f is the wave frequency and f_p is the spectral peak frequency.

and loss energy in breaking wave trains. For example, the amplitude difference in the low-frequency band of all nonbreaking wave trains, indicates a small energy decrease downstream while the free-wave amplitudes in the low-frequency band of all breaking wave trains slightly increase after the breaking (see Figs. 9 and 10).

Based on the error analysis and measured results, we remark that the errors made in the measurements and data analysis will not fundamentally change the results of energy loss and gain due to wave breaking.

5. Energy dissipation due to wave breaking

The free-wave amplitude spectra before and after the breaking of a transient wave train were respectively averaged for the two locations and four different runs. The differences between the average free-wave amplitude spectra of the wave train P3 before and after the breaking are shown as a function of the frequency normalized by the spectral peak frequency in Fig. 9. To provide a reference, the average free-wave amplitude spectrum
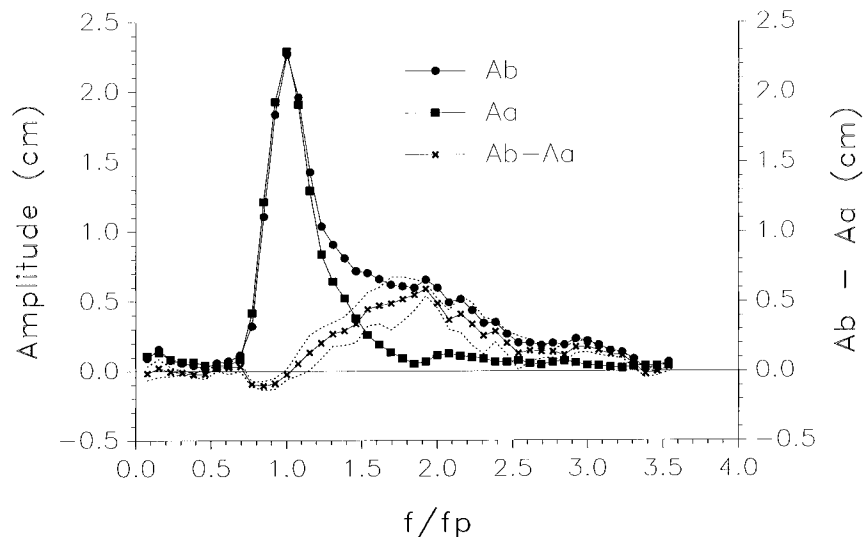

FIG. 9. Averaged free-wave elevation spectra, before (Ab) and after (Aa) a plunging breaker, and their difference spectrum ($Ab - Aa$). The dotted lines represent the 95% confidence interval ($\pm 2\sqrt{\sigma_b^2 + \sigma_a^2}$) of the amplitude-difference spectrum. The spectral peak frequency $f_p = 0.63$ Hz and σ_b and σ_a are the standard deviations of the mean spectra before and after breaking, respectively.
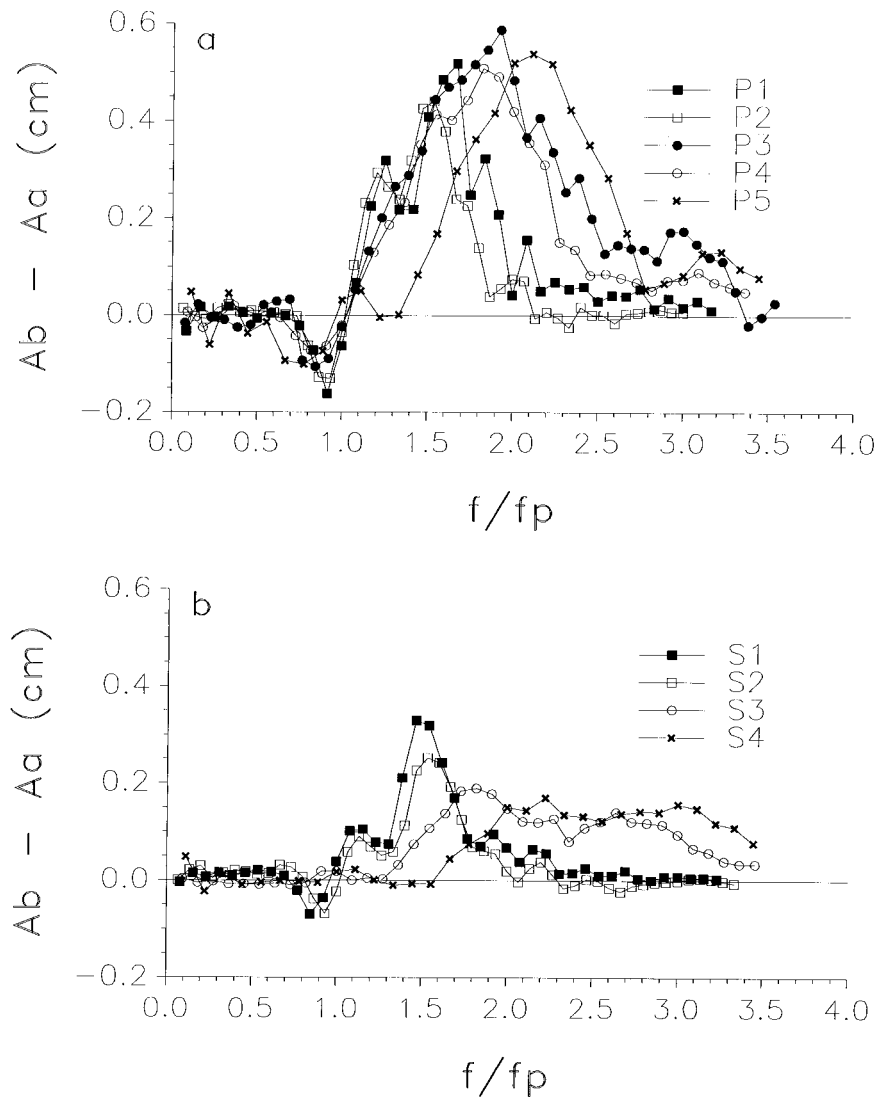
FIG. 10. Free-wave amplitude-difference spectra for (a) plunging and (b) spilling wave trains of Table 1: Ab and Aa are, respectively, the average free-wave amplitude spectra before and after breaking, f is the wave frequency, and f_p is the spectral peak frequency.

before and after the breaking of P3 are also plotted. Additionally, Fig. 9 shows the 95% confidence band ($\pm 2\sqrt{\sigma_b^2 + \sigma_a^2}$) of the amplitude-difference spectrum. However, the free-wave spectra 95% confidence bands, which are four times the standard deviation of the mean spectra ($\pm 2\sigma_b$ for before breaking and $\pm 2\sigma_a$ for after breaking), are not plotted to avoid too many lines.

The comparison of the free-wave amplitude spectra before and after the breaking shows that the free-wave amplitudes at the frequencies near and below the spectral peak frequency change a little, indicating that there is no significant energy loss or gain. On the other hand, all free-wave amplitudes in the frequency band ($f/f_p = 1.2–2.5$), significantly higher than the spectral peak frequency, become much smaller after the breaking. These observations are consistent with Rapp and Melville

(1990) and Kway et al. (1998), although their observations were based on the comparison of the resultant amplitude spectra. By carefully examining the difference in free-wave amplitudes before and after the breaking, it is observed that there is small energy loss at the frequencies slightly higher than the peak frequency and a small gain in the frequency band slightly below the peak frequency. Although the free-wave components near the spectral peak are the most energetic, the amplitude-difference spectrum shows that the energy loss is dominantly contributed from the free-wave components in the high-frequency band ($f/f_p = 1.2–2.5$). The loss (3–5 mm) is much greater than the uncertainties (or errors) ($\pm 2\sqrt{\sigma_b^2 + \sigma_a^2}$, 0.3–1.9 mm) in the high-frequency band. The amplitude-difference spectrum clearly shows energy gain in the low-frequency band.

Although the energy gain is very small, the uncertainties in the amplitude-difference spectrum in the low-frequency band are smaller. For example, at $f/f_p = 0.85$ the 95% confidence band of the amplitude difference, $(\pm 2\sqrt{\sigma_b^2 + \sigma_a^2})$, is ± 0.3 mm, much smaller than the measured energy loss (1 mm) at this frequency. The above observations further confirm that the measurement errors or uncertainties in the amplitude-difference spectrum are respectively much smaller than the energy loss or gain in the high- and low-frequency bands. The evidence of the energy gain supports an earlier observation of Melville (1996) that wave breaking could be the energy source to waves at very low frequencies.

To ensure the above observed trend of energy loss and gain with respect to wave frequency is general and not limited to the wave train P3, the corresponding results of all breaking wave trains studied are derived and summarized in Fig. 10. The amplitude-difference spectra before and after a plunging breaker and a spilling breaker are presented in Figs. 10a and 10b, respectively. The frequencies are normalized by their corresponding peak frequencies. Although the trend of energy dissipation with respect to normalized frequency varies in detail in different wave trains, three major features observed in Fig. 9 are found to be independent of the type of breaker. They are 1) dominant energy loss is contributed from the free-wave components in the high-frequency band (significantly higher than the peak frequency), 2) the energy loss or gain near the peak frequency is insignificant, and 3) a small energy gain occurs in the low-frequency band, below the spectral peak frequency. In comparing Fig. 10a and Fig. 10b, it is found that the energy loss of a plunging breaker is in general greater than that of a spilling breaker. This observation is expected from the intuition and also consistent with Rapp and Melville (1990) and Kway et al. (1998). It is also shown that the corresponding energy gain in the low-frequency band after a plunging breaker is in general greater than after a spilling breaker. The small energy gain in most transient wave trains studied is confined to the frequency band below the peak frequency. However, in three cases (P5, S3, and S4), the low-frequency band, which gains energy after the breaking, extends its upper boundary to slightly above the peak frequency although the center of the energy-gaining band is still significantly below the spectral peak. The extension of the upper boundary of an energy-gaining band possibly correlates to the center of the energy-losing (high-frequency) band located at the frequency much higher than the peak frequency.

Energy dissipation due to wave breaking dominantly contributed from the free-wave components of frequencies significantly higher than the peak frequency is not limited to the transient wave trains generated in flumes. It should be anticipated in ocean waves based on heuristic explanations. In an ocean wave field, free-wave components of different frequencies travel together, short-wavelength (high frequency) components ride on the surface of long-wave (low frequency) components and become shorter and steeper at the crests and longer and flatter at the troughs of long-wave components. This phenomenon is known as short-wave modulation by long waves and has been well documented (Phillips 1981; Longuet-Higgins 1987; Zhang and Melville 1990). When the crests of many free-wave components of different frequencies align, the local resultant wave elevation becomes extremely steep and may lead to wave breaking. Wave breaking, of both spilling and plunging breakers occurs at steep wave crests where short-wave components are located. This is why the energy loss in waves due to the breaking is at the expense of the short-wave components whose frequencies are higher than the peak frequency.

Most dissipated energy due to wave breaking transfers to the turbulence kinetic energy of seawater near the free surface (Rapp and Melville 1990; Thorpe 1993; Melville 1994). It is possible that a fraction of the dissipated energy of high-frequency free-wave components transfers to the energy of low-frequency free-wave components. It is of interest to find the ratio of the energy gain in the low-frequency free-wave components to the energy loss in the high-frequency free-wave components after an isolated breaker. As shown in Figs. 10a and 10b, the frequency bands of gaining and losing energy are clearly separated in the frequency domain. Hence, we may respectively compute the total loss in the high-frequency band and total gain in the low-frequency band by the integrations in the frequency domain. The low- and high-frequency bands were fixed as $f/f_p = 0.65$–1.0 and 1.0–3.25, respectively. The energy gain–loss ratio of each breaking transient wave train is presented in Table 1. It is found that the ratios of all breaking transient wave trains are substantially smaller than unity. The majority of them are indeed smaller than 15%. They also vary significantly for different wave trains, ranging from 6.4% to 26.7%. The average of all ratios is found to be about 12% and the median is 8.5%. The magnitude of the energy gain–loss ratio will be used to investigate the long-term evolution of ocean wave spectra in the next section.

In addition to presenting the differences in free-wave amplitudes as a function of the normalized frequency as in Fig. 10, we also plot energy dissipation or gain due to wave breaking against the phase velocity in Fig. 11, where the energy dissipation or gain are respectively normalized by the wave energy and phase velocity at the spectral peak. Figure 11 combines the results of plunging and spilling transient wave trains together. As expected, the figure shows that the trend of energy dissipation with respect to the normalized phase velocity is independent of the type of breakers. The energy loss is mainly in the range $C/C_p = 0.40$–0.95 and the small energy gain in the range $C/C_p = 1.03$–1.25. These observations again suggest that the gain and loss of energy during wave breaking are closely related to the spectral peak frequency (or phase velocity). It is also found that
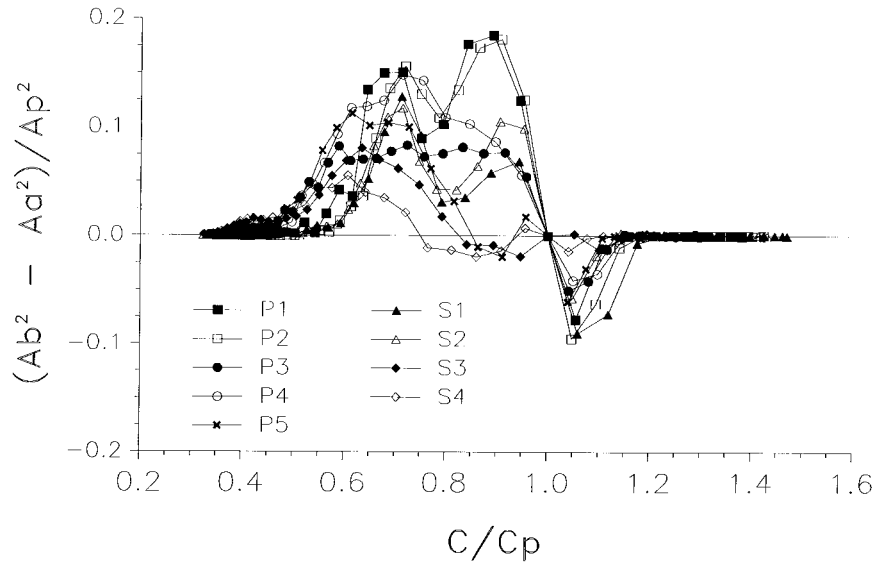
FIG. 11. Normalized free-wave energy dissipation spectra of the plunging and spilling wave trains of Table 1: Ab^2 and Aa^2 are, respectively, the average free-wave energy spectra before and after breaking, Ap^2 is the average spectral peak wave energy, C and C_p are the wave phase velocity and the peak's phase velocity, respectively.

the range of C/C_p for energy loss based on laboratory observations is consistent with field observations. Based on field observations of the dissipation of kinetic energy in the mixed layer and the incidence of wave breaking, Thorpe (1993) determined that the characteristic breaking event speed is much smaller than the dominant wave phase speed ($C/C_p = 0.25$). Melville (1994) using more recent field and laboratory measurements of the dissipation of kinetic energy in the mixed layer estimated that $C/C_p = 0.4$–0.63. Employing a novel acoustic instrument to track individual ocean breaking events Ding and Farmer (1994) showed that $C/C_p = 0.45$–0.75. Smith et al. (1996) using Doppler radar measurements of ocean wave groups and breaking waves found that $C/C_p = 0.8$. Their observations suggest that the wave breaking in the ocean is associated with the dominant wave and that the breaking (or energy dissipation) is from shorter waves ($C/C_p \ll 1.0$). The range of C/C_p for waves losing energy found in all above field observations except for Thorpe (1993) are virtually in the same range as shown in Fig. 11. This consistency confirms that the nondimensional variables used in the laboratory tests are relevant to ocean waves.

6. Implications to long-term evolution of ocean wave spectra

The long-term evolution of an ocean wave spectrum in space and time can be described by an energy transfer equation. In deep water and in the absence of currents it takes the form

$$\frac{\partial E}{\partial t} + \mathbf{\nabla} \cdot (\mathbf{C}_g E) = S_{\text{tot}}, \quad \text{and} \tag{1}$$

$$S_{\text{tot}} = S_{\text{in}} + S_{nl} + S_{\text{dis}},$$

where E denotes the wave energy density which is a function of the horizontal coordinates, time, wave frequency and direction, and $\mathbf{C}_g$ is the group velocity; S_{tot} is the total energy transfer rate, which consists of three parts; S_{in} stands for the source term regarding the energy input from wind, S_{nl} describes the rate of energy transfer between wave components of different frequencies owing to the nonlinear resonant (quartet) wave–wave interactions, and S_{dis} is the wave energy dissipation term due mainly to wave breaking.

So far the spectral representation of the dissipation term, S_{dis}, in the energy transfer equation has been empirically proposed. The third generation ocean wave models, such as the WAM Model (WAMDI Group 1988; Komen et al. 1994), use the following formulation to estimate S_{dis},

$$S_{\text{dis}} = C_{\text{ds}} \overline{\omega} \left(\frac{\omega}{\overline{\omega}} \right)^n \left[\frac{\hat{\alpha}}{\hat{\alpha}_{\text{PM}}} \right]^m E(\omega), \tag{2}$$

where

$$\hat{\alpha} = m_o \frac{\overline{\omega}^4}{g^2},$$

m_o denotes the zeroth moment of the spectrum, ω the radian wave frequency, and $\overline{\omega}$ the mean frequency of the spectrum. Here $\hat{\alpha}$ is related to the square of wave steepness and indicates the overall steepness of an ocean

wave field, and $\hat{\alpha}_{PM}$ is the value of $\hat{\alpha}$ when the spectrum of a wave field is of the Pierson–Moskowitz type. The parameters, C_{ds}, m, and n can be calibrated according to field measurements. The parameter n, was chosen to be 2 by Komen et al. (1984) and 4 by Janssen (1991). The product of parameters,

$$C_{ds}\,\overline{\omega}\left[\frac{\hat{\alpha}}{\hat{\alpha}_{PM}}\right]^m,$$

plays an important role in determining the total energy dissipation rate of a wave field but bears no effects on the energy dissipation rate as a function of wave frequency. The dependence of the dissipation rate on the frequency is essentially described by the kernel, $(\omega/\overline{\omega})\,{}^nE(\omega)$ in Eq. (2). The kernel indicates that the dissipation rate due to wave breaking is proportional to the magnitude of wave energy density at a frequency and to either the second (Komen et al. 1984) or fourth power (Janssen 1991) of the frequency.

The measurements reported in this study are the energy dissipation caused by an isolated breaker. Wave breaking at the sea surface usually occurs sporadically and irregularly. The energy dissipation of an isolated breaker is not the same as the dissipation rate of an ocean wave field. The former can be related to the latter when the probabilities of various types of breakers in an ocean wave field can be determined. However, it is noticed that the measurements of energy dissipation in all cases studied, regardless of spilling and plunging breakers, show a consistent trend of energy dissipation with respect to the normalized frequency. Thus, this general trend of the energy dissipation with respect to the frequency in transient wave trains is expected to be proportional to that of the dissipation rate in unidirectional ocean waves. The trend revealed from the measurements can be used to examine the empirical kernel used in the WAM regarding the dependence of the dissipation rate on the frequency. There are two striking differences between the trend revealed by our measurements and the kernel of the empirical formulation. First, the measurements show that there is almost no significant energy loss or gain in the frequency band near the spectral peak frequency, although the energy density is the largest there. This observation clearly contradicts the kernel that the energy loss rate at a frequency is proportional to the energy density at the frequency, indicating the kernel may be invalid to waves of frequencies near the peak frequency. The measurements also indicate that the energy loss during wave breaking comes mainly from the frequencies significantly higher than the spectral peak frequency. In the high-frequency band, the measurements seem to be consistent with the kernel that the energy loss increases with the increase in wave frequency and that the energy loss is related to the magnitude of the energy density. However, it needs more data and further analyses to determine the kernel function in the high-frequency band. Second, the small

energy gain at low frequencies is opposite to the kernel, which predicts a small energy loss rate. Although the magnitude of the measured energy gain in the low-frequency band is relatively small, it has important implications to the energy budget in the low-frequency band because there the energy input from wind is usually insignificant and the energy transfer from the high frequency band due to the nonlinear resonant wave interactions is relatively small as well.

The finding of the energy gain in the low-frequency band (mainly below the spectral peak frequency) due to wave breaking is crucial to the controversy regarding the energy imbalance in low-frequency ocean waves raised by Davidan and Lavrenov (1991). Utilizing the left hand side of Eq. (1), they estimated the total energy transfer rate as a function of frequency for different developed stages of ocean waves, ranging from steady-state waves at small fetches to almost fully developed wind-driven waves. In their computation, the local change in wave energy density is neglected ($\partial E/\partial t = 0$) because of the steady-state assumption, and the total energy transfer rate (S_{tot}) is hence determined solely by the "convective" term. The two-dimensional spectra used in their computation were approximately modeled and the parameters used to quantify the spectra of different developed stages of wind-driven waves were calibrated based on field measurements (Davidan et al. 1985). To study itemized energy transfer rates, they also respectively estimated the energy input rate from the wind (S_{in}) and the energy transfer rate due to nonlinear quartet resonance interactions (S_{nl}). The formulation given by Snyder et al. (1981) was used for the computation of S_{in} and the Boltzmann's integral expression (Hasselmann 1962) for S_{nl}. Hence, the formulas used in their computation of S_{in} and S_{nl} are similar to those used by the WAMDI group (1988). In comparing S_{tot} with S_{in} + S_{nl}, they found that there is a significant energy imbalance in the low-frequency band in all wave stages they studied. The imbalance indicates that S_{tot} is much greater than S_{nl} + S_{in} at the low-frequency range. To show the magnitude of the imbalance, their result of the energy transfer rates as a function of wave frequency of a nearly fully developed sea is reproduced in Fig. 12. For reference, the energy density spectrum is also plotted in the figure.

Figure 12 shows that S_{tot} is relatively large and positive at low frequencies (below the peak frequency) and close to zero at the frequencies significantly higher than the peak frequency. This implies that the spectral peak frequency will gradually downshift (toward a lower frequency) with the increase in the fetch length and that the energy density approximately reaches an equilibrium in the high-frequency band. The input from wind, S_{in}, is relatively large at high frequencies and diminishes to zero (negligible) at low frequencies, which is expected from the formulation of Snyder et al. (1981). The energy transfer rate due to nonlinear resonant interactions are positive in the low-frequency band and negative in the
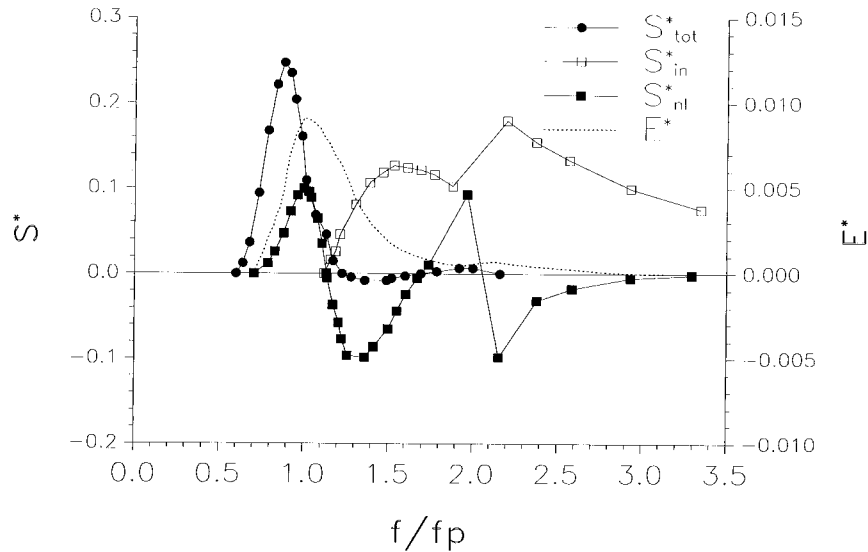
FIG. 12. Normalized source functions for a nearly fully developed fetch-limited sea: f is the wave frequency and S^* and E^* are, respectively, the transfer rate and the energy density normalized in terms of the gravity g, the friction velocity u_*, and the spectral peak frequency f_p; S^*_{tot} is the total energy transfer rate, S^*_{in} is the energy input by the wind and S^*_{nl} is the energy transfer by the nonlinear resonant (quartet) wave–wave interactions. The normalization is defined as $S^* = (g^2/u_*^4)S$ and $E^* = f_p(g^2/u_*^4)E$. This figure is reproduced from Davidan and Lavrenov's (1991) Fig. 4.

majority region of the high-frequency band, consistent with the result given by Hasselmann et al. (1985) and Komen et al. (1994). As shown in Fig. 12, S_{tot} is significantly greater than S_{nl} in the low-frequency band. Davidan and Lavrenov (1991) were not sure how to compute the dissipation rate S_{dis} and thus it was not computed. To quantify the differences between S_{tot} and S_{nl} in the low-frequency band, we respectively integrated S_{tot} and S_{nl} over the low-frequency band ($f/f_p = 0.55$–1.0). It is found that the integrated S_{nl} is only about 22% of the integrated S_{tot} when $S_{\text{dis}} = 0$ is assumed. If the dissipation rate, S_{dis}, was computed according to the formulation suggested in the WAM, the imbalance in the low-frequency range would be even greater.

The large energy imbalance at low frequencies raises a question: through which mechanism or from which source, energy is transferred to waves at low frequencies because the nonlinear energy transfer through resonance interactions accounts only for a small portion of the total energy increase rate of waves at low frequencies. Our laboratory observations suggest that wave energy can be gained at the low frequencies due to wave breaking at the expenses of energy loss of waves at high frequencies. To explore the possibility that wave breaking is the major energy source to waves of low frequencies, efforts were made to find whether or not the energy imbalance at the low frequencies can be approximately accounted by the energy gain at the low frequencies through the mechanism of wave breaking. A rough estimate of the energy gain rate in the low-frequency band

due to wave breaking was made based on our measurements.

As shown in Fig. 12, $S_{\text{tot}} \simeq 0$ in the high-frequency band, indicating that the energy density in the frequency band significantly higher than the peak spectral frequency is approximately in equilibrium. Hence, the dissipation rate in the high-frequency band can be deduced by $S_{\text{dis}} \simeq -(S_{\text{in}} + S_{\text{nl}})$. Consequently, the energy dissipation rate in the high-frequency band was calculated by integrating $-(S_{\text{in}} + S_{\text{nl}})$ over the frequency band ($f/f_p = 1.30$–3.35). Based on our measurements (see Table 1), the average gain–loss ratio is about 12%. Assuming the energy dissipation in the high-frequency band was mainly caused by wave breaking, the energy gain rate in the low-frequency band ($f/f_p = 0.55$–1.0) can then be obtained by multiplying the integrated S_{dis} in the high-frequency band with the average ratio (12%). The estimated energy gain rate in the low-frequency band due to wave breaking turned out to be about 50% of the integrated total energy gain rate (S_{tot}) in the low-frequency band and is more than twice of the integrated energy transfer rate S_{nl} resulting from resonant quartet interactions. The above estimate shows that the energy gain is in the same order of the energy imbalance calculated by Davidan and Lavrenov (1991). Although the above estimate is rough and further studies are required to quantify the energy gain in waves of low frequencies, we remark that wave breaking is likely a major energy source to ocean waves at low frequencies, which has not been considered in current ocean wave models.

It is worth mentioning that wind gustiness, the other major source possibly contributing to the total energy gain of waves at low frequencies, had been proposed by Davidan and Lavrenov (1991). Specially in the later stages of wave growth, it was thought that the growth of low-frequency waves can be greatly affected by wind gustiness (Komen et al. 1994). The effects of gustiness on the growth of waves at low frequencies were quantified by Nikolayeva and Tsimring (1986) and more recently by Miles and Ierley (1998). Nikolayeva and Tsimring (1986) indicated a considerable enhancement of energy transfer due to gustiness to low-frequency waves in well-developed wind-driven waves. Miles and Ierley (1998), however, found that in well-developed wind-driven waves the energy input from wind gustiness to low-frequency waves is only about 1/80 of that predicted by Nikolayeva and Tsimring and actually smaller than that predicted by Miles (1959). Therefore, based on the study of Miles and Ierley (1998) wind gustiness is not likely to be a candidate to provide significant energy to waves of low frequencies.

7. Conclusions and future work

The HWM was used to decouple the bound-wave components from the measured wave elevations. Because of the exclusion of bound-wave components, the free-wave amplitude spectra of steep transient wave trains are almost steady in the absence of wave breaking and within a short distance. Different from the comparison of the resultant amplitude spectra (Rapp and Melville 1990; Kway et al. 1998), the dependence of energy dissipation on wave frequency in breaking waves can be more accurately determined by comparing the free-wave amplitude spectra before and after an isolated breaker. The energy dissipations due to various isolated breakers show a consistent pattern with respect to wave frequency. First, wave breaking in an irregular wave field consisting of many free-wave components mainly consumes energy of those frequencies significantly higher than the spectral peak frequency. Second, wave components of frequencies close to the spectral peak frequency lose or gain insignificant energy during wave breaking although their energy density is the greatest among all wave components in an irregular wave field. Finally, wave components of frequencies below the spectral peak gain a small portion (about 12%) of energy lost by the wave components of high frequencies. These findings contradict current empirical formulas used for determining wave dissipation due to wave breaking. They have important implications to the ocean wave energy budget, specially to the energy growth rate of wave components at frequencies below and near the spectral peak frequency.

Our experimental study probably is the first attempt to estimate the energy gain in the low-frequency band in terms of the energy loss in the high-frequency band in a transient wave train containing an isolated breaker.

However, the effort to quantify analytically how much energy can be transferred to low-frequency waves from breaking high-frequency waves was made three decades ago. Longuet-Higgins (1969) proposed a mechanism called ''maser'' to compute the energy gain due to short-wave breaking over a periodic long wave. Nevertheless, Hasselmann (1971) showed that the work done on the long wave by the breaking of short waves through the maser mechanism was balanced by the loss of potential energy arising from the mass transport. Hence, the breaking short waves could not provide the energy to long waves through the maser mechanism. Melville (1996) suggested that the transfer of energy to low-frequency waves could be due to the release of free-long-wave components resulting from the change in the gradients of the radiation stress accompanying breaking, but failed to render a quantitative relation between the changes in the radiation stress and energy gain in low-frequency waves. It seems that the understanding of how energy is transferred to low-frequency waves during breaking is still a challenging task and requires further investigation.

Wave breaking in deep or intermediate-depth water usually occurs when local wave energy exceeds a certain level due to the crest alignment of a great number of free-wave components. While in shallow water, wave breaking may be induced by shoaling effects. Because wave breaking in our measurements was generated by a wave focusing technique, our results may be only relevant to the wave breaking in deep or intermediate-depth water. Also due to the limitation of 2D flumes, the results presented here may not be valid if the directions of the high-frequency band and low-frequency band of an ocean wave field are quite different. It is of great interest to study the energy dissipation of directional wave breaking in a large three-dimensional wave basin.

REFERENCES

Anis, A., and J. N. Moum, 1995: Surface wave–turbulence interactions: Scaling $\varepsilon(z)$ near the sea surface. *J. Phys. Oceanogr.,* **25,** 2025–2045.

Banner, M. L., and D. H. Peregrine, 1993: Wave breaking in deep water. *Annu. Rev. Fluid Mech.,* **25,** 373–397.

Cao, P., and J. Zhang, 1997: Slow motion response of compliant offshore structure. *J. Offshore Polar Eng.,* **7,** 119–126.

Couch, A. T., and J. P. Conte, 1997: Field verification of linear and nonlinear hybrid wave models for offshore tower response prediction. *J. Offshore Mech. Arct. Eng.,* **119,** 158–165.

Davidan, I. N., and I. V. Lavrenov, 1991: On energy imbalance in the low-frequency region of developed wave spectrum. *Izv. Atmos. Oceanic Phys.,* **27,** 604–610.

——, L. I. Lopatukhin, and V. A. Rozhkov, 1985: *Vetrovoye Vol-neniye v Mirovom Okeane* (Wind waves in the world ocean). Gidrometeoizat, Leningrad.

Ding, L., and D. M. Farmer, 1994: Observations of breaking surface wave statistics. *J. Phys. Oceanogr.,* **24,** 1368–1387.

Drennan, W. M., M. A. Donelan, E. A. Terray, and K. B. Katsaros, 1996: Oceanic turbulence dissipation measurements in SWADE. *J. Phys. Oceanogr.,* **26,** 808–815.

Hasselmann, K., 1962: On the nonlinear energy transfer in a gravity wave spectrum. Part 1: General theory. *J. Fluid Mech.,* **12,** 481–500.

——, 1971: On the mass and momentum transfer between short gravity waves and larger-scale motions. *J. Fluid Mech.,* **50,** 189–205.

Hasselmann, S., K. Hasselmann, J. H. Allender, and T. P. Barnett, 1985: Computations and parameterizations of the nonlinear energy transfer in a gravity–wave spectrum. Part II: Parameterizations of the nonlinear energy transfer for application in wave models. *J. Phys. Oceanogr.,* **15,** 1378–1391.

Janssen, P. A. E. M., 1991: Quasi-linear theory of wind wave generation applied to wave forecasting. *J. Phys. Oceanogr.,* **21,** 1631–1642.

Komen, G. J., S. Hasselmann, and K. Hasselmann, 1984: On the existence of a fully developed wind-sea spectra. *J. Phys. Oceanogr.,* **14,** 1271–1285.

——, L. Cavalieri, M. Donelan, K. Hasselmann, S. Hasselmann, and P. A. E. M. Janssen, 1994: *Dynamics and Modeling of Ocean Waves.* Cambridge University Press, 532 pp.

Krafft, M. J., and C. H. Kim, 1987: Extreme transient water wave generation at Texas A&M University. COE Rep. 294, 63 pp. [Available from COE Division, Texas A&M University, College Station, TX 77843.]

Kway, J. H., Y. Loh, and E. Chan, 1998: Laboratory study of deep-water breaking waves. *J. Ocean Eng.,* **25,** 657–676.

Longuet-Higgins, M. S., 1969: A nonlinear mechanism for the generation of sea waves. *Proc. Roy Soc. London,* **311A,** 371–389.

——, 1987: The propagation of short surface waves on longer gravity waves. *J. Fluid Mech.,* **177,** 293–306.

Melville, W. K., 1994: Energy dissipation by breaking waves. *J. Phys. Oceanogr.,* **24,** 2041–2049.

——, 1996: The role of surface-wave breaking in air–sea interaction. *Annu. Rev. Fluid Mech.,* **28,** 279–321.

Meza, E., J. Zhang, and R. J. Seymour, 1999: Prediction of surface wave elevation based on pressure measurements. *J. Offshore Mech. Arct. Eng.,* **121,** 242–250.

Miles, J. W., 1959: On the generation of surface waves by shear flows, Part 2. *J. Fluid Mech.,* **6,** 568–582.

——, and G. Ierley, 1998: Surface-wave generation by gusty wind. *J. Fluid Mech.,* **375,** 21–28.

Nikolayeva, Y. I., and L. S. Tsimring, 1986: Kinetic model of the wind generation of waves by a turbulent wind. *Izv. Atmos. Oceanic Phys.,* **22,** 102–107.

Phillips, O. M., 1979: Surface wave physics—A survey. Flow Res. Rep. 107, 91 pp.

——, 1981: The dispersion of short wavelets in presence of a dominant long wave. *J. Fluid Mech.,* **107,** 465–485.

——, 1984: On the response of short ocean wave components at a fixed wavenumber to ocean current variations. *J. Phys. Oceanogr.,* **14,** 465–485.

Randall, R. E., J. Zhang, and J. K. Longridge, 1993: Laser Doppler anemometer measurements of irregular water wave kinematics. *Ocean Eng.,* **20,** 541–554.

Rapp, R. J., and W. K. Melville, 1990: Laboratory measurements of deep-water breaking waves. *Philos. Trans. Roy. Soc. London,* **331A,** 735–800.

Smith, M. J., E. M. Poulter, and J. A. McGregor, 1996: Doppler radar measurements of wave groups and breaking waves. *J. Geophys. Res.,* **101,** 14 269–14 282.

Snyder, R. L., F. W. Dobson, J. A. Elliott, and R. B. Long, 1981: Array measurements of atmospheric pressure fluctuations above surface gravity waves. *J. Fluid Mech.,* **102,** 1–59.

Spell, C. A., J. Zhang, and R. E. Randall, 1996: Hybrid wave model for unidirectional irregular waves—Part II: Comparison with laboratory measurements. *Appl. Ocean Res.,* **18,** 93–110.

Sue, M. Y., and R. E. Green, 1981: Experimental studies of strong nonlinear interactions of deep-water gravity waves. *Wave Dynamics and Radio Probing of the Ocean Surface,* O. M. Phillips and K. Hasselmann, Eds., Plenum, 231–253.

Terray, E. A., M. A. Donelan, Y. C. Agrawal, W. M. Drennan, K. K. Kahma, A. J. Williams III, P. A. Hwang, and S. A. Kitaigorodskii, 1996: Estimates of kinetic energy dissipation under breaking waves. *J. Phys. Oceanogr.,* **26,** 792–807.

Thorpe, S. A., 1993: Energy loss by breaking waves. *J. Phys. Oceanogr.,* **23,** 2498–2502.

WAMDI Group, 1988: The WAM model—A third generation ocean wave prediction model. *J. Phys. Oceanogr.,* **18,** 1775–1810.

Yuen, H. C., and B. M. Lake, 1982: Nonlinear dynamics of deep-water gravity waves. *Adv. Appl. Mech.,* **22,** 67–229.

Zhang, J., and W. K. Melville, 1990: Evolution of weakly nonlinear short waves riding on long gravity waves. *J. Fluid Mech.,* **214,** 321–346.

——, L. Chen, M. Ye, and R. E. Randall, 1996: Hybrid wave model for unidirectional irregular waves—Part I: Theory and numerical scheme. *Appl. Ocean Res.,* **18,** 77–92.